Hydrogen production from solar thermal dissociation of natural gas: development of a 10 kW solar chemical reactor prototype

Sylvain RODAT*, Stéphane ABANADES, Jean-Louis SANS, Gilles FLAMANT

Processes, Materials, and Solar Energy Laboratory, CNRS (PROMES-CNRS, UPR 8521), 7 Rue du Four Solaire, 66120 Odeillo Font-Romeu, France

Abstract:

This study addresses the solar thermal decomposition of natural gas for the co-production of hydrogen, as well as Carbon Black as a high-value nano-material, with the bonus of zero CO_2 emissions. The work focused on the development of a medium-scale solar reactor (10 kW) based on the concept of indirect heating. The solar reactor is composed of a cubic cavity receiver (20 cm side), which absorbs concentrated solar irradiation through a quartz window via a 9 cm-diameter aperture. The reacting gas flows inside four graphite tubular reaction zones that are settled vertically inside the cavity. Experimental results were as follows: methane conversion and hydrogen yield of up to 98% and 90%, respectively, were achieved at 1770K, and acetylene was the most important by-product, with a mole fraction up to about 5%. The effect of the methane mole fraction in the feed gas, the residence time and the temperature on the reaction extent was analyzed. In addition to the experimental section, thermal simulations were carried out. They showed a homogeneous temperature distribution inside the cavity receiver of the reactor and permit to draw up a thermal balance.

Keywords: Hydrogen production; Solar thermal energy; Methane dissociation; Solar reactor; Thermal simulation.

* Corresponding author. Fax: +33 4 68 30 29 40.
E-mail address: sylvain.rodat@promes.cnrs.fr

1. Introduction

Abundant carbon emissions in the atmosphere result in global warming. Fossil energy resources are decreasing and global conventional oil production is expected to peak within 20 years, while the peak production for natural gas could occur by 2050 (Mason, 2007). In the near to medium-term future, however, fossil fuels (especially natural gas) will continue to play a major role (Barreto et al., 2003). The decarbonization of energy is a solution for a more sustainable energy policy based on hydrogen. It is also important to use renewable energy in order to avoid further CO_2 emissions in the process. In the present work, the solar thermal decomposition of methane into carbon and hydrogen in the absence of catalyst is studied. This process, which is also called "direct decarbonization" by Muradov (2001a), produces two valuable products: hydrogen as a clean energy carrier and Carbon Black (CB) as a high-value nanomaterial.

If 50% of all natural gas available in the US were converted into H_2 and CB via methane cracking, it would produce 40 Mt of carbon (Muradov et al., 2005b); the annual world CB production is about 9 Mt (Adams, 2007). Muradov (2005b) proposed a path toward a hydrogen-carbon economy and has suggested new markets for CB, such as in building and construction materials, the production of electricity using direct carbon fuel cells, and soil amendment. However, another approach could be to replace only the CB production by solar methane cracking. Dahl et al. (2004b) showed that 1650 solar chemical plants of 16.6 MW_{th} (each producing 1600 tons/year H_2 and 5000 tons/year CB) would be sufficient to satisfy the world CB demand. The economics of the process depend on the CB properties. The selling price of H_2 is determined to be \$13.80/GJ for achieving a 15% IRR (Internal Rate of Return) when CB is sold at \$0.66/kg. For a CB selling price of \$0.80/kg, the price of H_2 for achieving the 15% IRR drops to \$10/GJ. With CO_2-equivalent Avoidance Credits, the economics of the process can be further improved (Wyss et al., 2007). For this scenario, by replacing conventional furnace black processing, the solar-thermal process avoids the consumption of 277 MJ of fossil fuel and the emission of 13.9 kg-equivalent CO_2/kg H_2 produced as compared to conventional steam-methane reforming and furnace black processing. Thus, methane cracking is proposed as a transition process toward a renewable-based hydrogen economy.

Methane decomposition can be described by the following overall reaction (1):

$$CH_4 \rightarrow 2H_2 + C \qquad (1)$$

ΔH° = 75 kJ mol^{-1} (216 kJ mol^{-1} for CH_4 at 298 K and products at 2000 K)

Kinetic studies show very variable activation energy values depending on the type of reactor, the gas residence time and temperature, and the presence of catalyst. For example, a value of 404 kJ/mol was selected for the simulation of methane cracking in a three-phase plasma pilot reactor (Gonzalez-Aguilar et al., 2004). In a fluidized bed composed of CB, the activation energy determined by Muradov (2005a) was smaller (205–236 kJ/mol). Indeed, the presence of carbon particles has a catalytic effect (Muradov, 2001b) and decreases the activation energy. Work was also conducted in order to determine a reaction mechanism. Holmen et al. (1995) and Guéret and Billaud (1994) especially discussed the production of C_2 hydrocarbons by methane pyrolysis. In particular, they showed the importance of the dilution of methane by hydrogen to increase the production of acetylene. A stepwise dehydrogenation with intermediates ethane (C_2H_6), ethene (C_2H_4), and acetylene (C_2H_2) is the commonly accepted chemical mechanism.

The thermal decomposition of methane can be conducted in solar chemical reactors based on two different concepts for reactant heating: direct and indirect heating. In the first case (direct heating), heat is directly absorbed by particles and the reactor can be seeded to increase radiant absorption and nucleation sites. This method was studied by Kogan and Kogan (2003), who applied a tornado flow configuration to prevent deposition of particles onto the window. In this configuration, an auxiliary flow of protecting gas is introduced at the periphery of the window and is directed towards the window central area. It is accelerated by the negative pressure gradient generated by the free vortex flow. The auxiliary boundary layer flow at the window surface is thereby stabilized and remains attached to the surface all the way to the center of the window. Thus, the window is kept clear. Experimental studies focused first on an unseeded reactor in which a 28% extent of reaction was reached with temperatures of up to 1320K. The development of a seeded reactor was also reported: it concerned the determination of powder seeding conditions under which the reactor window is perfectly screened (Kogan et al., 2004) and the development of a powder seeding device (Kogan et al., 2005). A vortex flow reactor laden with carbon particles that serve as radiant absorbers and nucleation sites was also experimented by Hirsch and Steinfeld (2004). Their maximum chemical conversion of CH_4 to H_2 was 67% at 1600K and 5 kW power. The feasibility of such a reactor was demonstrated and was proposed as a transition path toward solar hydrogen. Moreover, a tubular, nozzle-type solar reactor (1 kW) was studied by Abanades and Flamant (2007). The conversion of CH_4 led to a yield of H_2 exceeding 97% and 90%, respectively, for a wall temperature of 1660K and a system without the injection of carbon particles. The main secondary hydrocarbon identified was acetylene

(with a mole fraction up to 5%). Increasing the temperature and the specific surface area available for the reaction showed a positive effect on the reaction extent. The wall surface reaction was the controlling chemical mechanism.

The difficulty of cleaning the window can be avoided by using indirect heating at the expense of further heat losses during heat transfer. Indirect heating avoids particle deposition on the window as a result of the reaction. Indeed, the presence of particles can be critical if they deposit on the window, causing over-heating and possible window breakage. A fluid-wall aerosol flow reactor was tested by Dahl et al. (2004a). Results showed 90% methane conversion at 2133K and high quality carbon was produced. Nevertheless, a low thermal efficiency was highlighted due to reradiation losses, cooling zones and optical losses in the visible spectrum from the secondary concentrator.

These different works have shown the feasibility of efficient methane decomposition in laboratory-scale solar reactors. The next step up would be to propose a scaled-up solar reactor prototype design suitable for the solar thermal dissociation of methane.

The objective of the study is to present recent work on the experimental testing of a 10 kW solar reactor prototype (SR10), based on the concept of indirect heating. Preliminary experiments were first conducted in a reactor featuring two concentric graphite tubes heated by an external plasma flow. The gas entered the inner tube and flowed back through the annular space of the outer tube, heated by the hot walls of the tube (via conduction and IR radiation). Complete methane decomposition was reached (X_{CH4} = 100%) at 1985K and the H_2 yield was in the range of 80-95%. Thus, this concept was extended to the solar reactor prototype SR10. This 10 kW reactor is composed of four tubes with a design similar to that tested with the plasma source.

2. Experimental set-up

2.1. Reactor design

The reactor (presented in Figure 1) is composed of a blackbody-cavity that receives the concentrated solar radiation, which enters via a 9 cm-diameter aperture, and of four tubular reaction zones in which the reactive gas flows. A quartz window, swept by a nitrogen flow, lets solar radiation enter the cavity and separates the inside cavity from the ambient oxidizing atmosphere. The reaction takes place in the four tubular graphite sections that are placed in the cubic, 20 cm-side graphite cavity receiver (solar absorber). Each reaction zone is

composed of two concentric graphite tubes. The gas enters the inner tube and flows out by the annular space between the outer and inner tubes. This design permits the gas residence time to increase and the reactants to preheat. The inner tube diameters are 12 mm o.d. and 4 mm i.d. The outer tube diameters are 24 mm o.d. and 18 mm i.d. (configuration A). In addition, other tube configurations were tested in order to increase the residence time and to delay carbon deposition. In no case was the external tube changed. (Figure 2):

Configuration B: internal graphite tube 12x4 mm with 7 mm drilling in the second half; this configuration allowed the residence time to increase in the hottest part of the tube.

Configuration C: internal graphite tube 12x4 mm with external milling; this configuration was supposed to delay tube blocking by increasing the annular space where the carbon deposit occurs.

Configuration D: internal alumina tube 12x8 mm (idem configuration A with 8 mm i.d. instead of 4 mm); this configuration was tested in order to study the influence of the material.

The heated tube length inserted into the graphite cavity is about 160.5 mm; the remaining length (about 200 mm) corresponds to the insulation zone. The reactor cavity is insulated by three different insulating materials to lower conduction losses, forming an insulation layer of 15 cm (5 cm for each insulating material). Table 1 gives their maximum operation temperatures and thermal conductivities. Insulating material 1 constitutes the first insulation layer around the graphite cavity since it exhibits the highest temperature of operation. The surrounding outer shell of the reactor is made of stainless steel. The steel box size is 535x535x373 mm. The front face is made of aluminum alloy. An aperture plate made in copper holds the quartz window and a copper component is used for the gas injection and collection on the top of the reactor. The front face, the aperture plate and the copper component are water-cooled.

The reactor is designed for a nominal power of 10 kW and is placed at the focus of the 1 MW solar furnace of the CNRS-PROMES laboratory (Figure 3). The furnace is composed of a field of 63 heliostats at full power (45 m² per heliostat) and of a parabolic concentrator (1830 m^2) delivering up to 9000 suns at the focal plane. During experiments on the 10 kW scale, only a fraction of the parabola is used by limiting the number of heliostats involved.

2.2. Experimental equipment and procedure

The gas mixture (argon and methane) is introduced in each tube with a controlled composition. Two mass-flow meters are used per graphite tube to control the flow-rates of Ar and CH_4 (Brooks Instruments model 5850 S, range 0-10 NL/min for methane and 0-20 NL/min for argon, precision 0.7% of the measurement +/-

0.2% of the full scale). The gas composition entering each tubular reaction zone can then be controlled with accuracy. The temperature is measured by a solar-blind optical pyrometer (wavelength: 5.14 μm) through CaF_2 windows and by type S and K thermocouples. A maximum temperature up to 2000K is expected to obtain both high methane conversion and high grade CB. The gases are cooled at the exit and then flow through a filter bag to separate carbon particles. The filter bag (diameter: 127 mm, length: 800 mm) is made of Ryton with a Mikrotex membrane (type 3601-57, 500 g/m²). The operation under reduced pressure (about 40 kPa) is enabled thanks to the use of a vacuum pump (P6010 SI32-3X4, feed pressure 4 bars, maximum vacuum flow of 3.2 NL/s at -40 kPa). This permits the delay of carbon clogging in the tubes. To monitor the absolute pressure, each tube entry is equipped with a pressure controller with a ceramic cell. The measurement scale is 0-4 bars and the precision is +/- 0.30% of the full scale.

The first experimental step is the heating of the reactor under an argon flow in the tubes. Once the desired temperature is reached, the mixture of argon and methane is injected with a controlled composition. An acquisition system permits the saving of different data, such as temperatures, pressures, and gas species concentrations (H_2 and CH_4). The continuous analysis of methane and hydrogen is enabled by a specifically devoted gas analyzer (NGA 2000 MLT3); the methods used for H_2 and CH_4 analysis are thermal conductivity and infrared detection, respectively. The resolution is 1% of the full scale. The measurement of CH_4 concentration is used for interference compensation in the measurement of H_2. The analyzer is equipped with appropriate internal components (pump, filter and sample flow-meter) to provide a suitable gas sampling to the measurement cells. A gas chromatograph (GC) also measures online the outlet concentrations of methane, hydrogen, ethane, ethene, and acetylene. The gas outlet is connected to a nearby micro GC (Varian CP 4900) equipped with Thermal Conductivity Detectors (TCD) and two columns. A bypass stream to be analyzed is aspirated through a set including a primary sampler (peristaltic pump) and a secondary sampler (internal pump of the GC). The micro GC is equipped with 2 channels: Channel 1 (MolSieve 5A PLOT 10M Backflush) for H_2, N_2, O_2, CO, CH_4; Channel 2 (PoraPLOT U 10M Backflush) for species such as CH_4, C_2H_6, C_2H_4, C_2H_2, as well as H_2. The carrier gas used for chromatography analysis is argon, which is also used as buffer gas during methane cracking experiments, thereby eliminating matrix effects.

The positions of temperature measurements are defined in Figure 4. The pyrometer is directed toward a tubular reaction zone, while three thermocouples measure the temperature at three different positions: one is in contact with the graphite cavity (thermocouple 1), one is settled between the first and the second insulation layers (thermocouple 2), and one is between the second and the third insulation layers (thermocouple 3).

Calorimetric measurements were also performed to determine the real power entering the reactor aperture: it was determined to be about 15 kW under nominal conditions.

2.3. Experimental conditions

Experimental runs (17) were carried out with methane injection, enabling hydrogen production from methane cracking. Table 2 summarizes the different experimental conditions tested. The gas residence time is calculated by dividing the volume of the tubular reaction zones inserted into the graphite cavity by the total volumetric gas flow-rate at the tube temperature and pressure. This calculation does not take into account the moles of species created by the reaction, but it provides a characteristic residence time for the reactor hydrodynamic. The temperature of the tubes varied between 1670 and 1770K, the mole fraction of methane in the feed varied between 10 and 33%, and the total methane flow-rate varied between 1.2 and 8 NL/min.

Typical results concerning temperature measurements are presented for run 2, which was conducted at a temperature of 1770K and a pressure of 38 kPa. Figure 5 shows the time course of temperatures in the reactor given by the three thermocouples. Time zero corresponds to the start of heating. The DNI (Direct Normal Irradiation) is quite stable throughout the experiment (about 1000 W/m², typical of a good sunny day). The complete thermal steady state was not reached in the whole reactor since the temperatures measured in the insulating material (5 cm and 10 cm away from the graphite cavity) were not stable during the methane cracking experiment. Thermal transient simulations performed with Fluent software show that a day of constant irradiation is not sufficient to reach steady temperature in the insulating zone. However, the period of methane cracking corresponds to a period of constant temperature of the cavity wall (thermocouple 1). In addition, the temperatures given by thermocouple 1 and by the pyrometer are similar. This confirms that the whole cavity can be considered isothermal with a homogeneous temperature of the tubes and the cavity walls.

3. Experimental results and discussion

3.1. Overview

The main results are listed in Table 3.

CH_4 conversion is defined by: $$X_{CH_4}=\frac{F_{0,CH_4}-F.y_{CH_4}}{F_{0,CH_4}} \quad . \tag{2}$$

H_2 yield is calculated from: $$Y_{H_2}=\frac{F.y_{H_2}}{2.F_{0,CH_4}}, \tag{3}$$

where F_{0,CH_4} is the inlet molar flow-rate of CH_4, y_i is the mole fraction of species i, and F is the total outlet flow-rate (with argon as buffer gas) obtained from:

$$F=F_{Ar}+F.y_{CH_4}+F.y_{H_2}+F.y_{C_2H_2}+F.y_{C_2H_4}+F.y_{C_2H_6} \quad . \tag{4}$$

Reactor thermo-chemical efficiency is given by:

$$\eta_{ch} = F_{0,CH_4}.X_{CH_4}.\Delta H_{Reactants(298K)\rightarrow Products(Treactor)}/P_{solar} \quad , \tag{5}$$

where F_{Ar} is the molar flow-rate of argon, F_{0,CH_4} is the inlet molar flow-rate of methane, X_{CH_4} is the chemical conversion, ΔH is the enthalpy change of the reaction when the reactants are fed at 298K and the products are obtained at $T_{reactor}$, and P_{solar} is the solar power input (W).

Table 3 indicates the reactor performances for different operating conditions. The maximum methane conversion and hydrogen yield reached were 98% and 90%, respectively, at 1770K (experimental conditions 1). The main by-product of the decomposition reaction was acetylene, with a mole fraction up to 5%. Thermochemical efficiencies up to 5% were achieved, but they can be further improved by increasing the methane content in the feed gas. The influence of three main parameters, the methane mole fraction in the feed gas, the residence time, and the temperature was especially considered.

3.2. Influence of the methane mole fraction

Figure 6 presents the time evolution of CH_4 and H_2 mole fractions in the off-gas obtained with experimental conditions 3 and 4. Time zero corresponds to methane injection. These experiments were carried out with 16 NL/min and 20 NL/min of argon respectively (constant CH_4 flow-rate of 4 NL/min, mean

temperature of 1770 K, and pressure of 35 kPa). The residence time was 17 ms down to 14 ms. The H_2 mole fraction was 27% with 16 NL/min of argon down to 23% with 20 NL/min of argon. The CH_4 conversions were 97% and 94%, respectively. It appears that decreasing the CH_4 mole fraction via dilution tends to decrease CH_4 conversion.

Results concerning the time evolution of CH_4 and H_2 mole fractions for experiments 13, 14, 15 are plotted in Figure 7. Time zero corresponds to the start of methane injection. The total gas flow-rate was maintained constant at 20 NL/min (residence time of 18 ms) and the CH_4 mole fraction was increased (10%, 20%, and 30%, respectively). The operating temperature was 1740K. Three different levels can be identified on the concentration curves corresponding to each experimental condition of CH_4 mole fraction in the feed gas. An increase of the methane mole fraction in the feed results in an increase of the hydrogen and methane mole fractions in the off-gas.

Figure 8 plots the CH_4 conversion and the H_2 yield as a function of the CH_4 mole fraction for experiments 13, 14, and 15 (triangle marks). The mole fraction of methane varied between 10% and 30%, whereas the CH_4 conversion and H_2 yield were quite constant at about 80% and 60%, respectively. Similar experiments (10, 11, and 12) were conducted at a lower temperature (1670K) and gave the same trend (square marks). Thus, for a given residence time, the CH_4 conversion and the H_2 yield do not vary significantly when increasing the CH_4 mole fraction. This implies that the thermochemical efficiency can be greatly improved by increasing the CH_4 mole fraction.

Assuming a first order kinetic expression (Trommer et al., 2004) and an ideal plug flow reactor model, the residence time τ can be calculated from (Abanades and Flamant, 2008):

$$k\tau = -(1+\alpha)\beta\ln(1-X_{CH_4}) - \alpha\beta X_{CH_4}\,, \tag{6}$$

where k is the kinetic rate constant, following the Arrhenius law:

$$k = k_0 . \exp(-E_a / RT)\,. \tag{7}$$

For each run, it is possible to estimate the kinetic rate constant, k. The mean k was 56.4 s^{-1} at 1670K (runs 10 to 12) and 102.2 s^{-1} at 1740K (runs 13 to 15). At a given temperature, the variation of k around the mean value from one run to another was less than 8%. The weak variation of the kinetic rate constant means that the gas temperature change may not be significant when increasing the methane mole fraction. Indeed, radiation absorption by methane and by the CB particles improves heat transfer to the gas phase when the methane concentration increases. A higher CH_4 concentration also results in a higher H_2 concentration, thus increasing the

thermal conductivity of the gas mixture. Both phenomena contribute toward heating of the gas when the inlet content of methane increases. Thus, the addition of methane does not cause a significant temperature decrease, which explains why the conversion remains unchanged. The reaction seems to be limited by kinetics. By assimilating the gas temperature to the tube wall temperature, the kinetic parameters were estimated to be: k_0=1.47 10^8 s^{-1} and E_a=205 kJ/mol.

3.3. Influence of the residence time

Considering ideal gas behavior, the residence time is affected by three parameters: the temperature, the pressure, and the molar gas flow-rate. A temperature decrease is not a good way to increase the residence time, since it will negatively affect the reaction kinetics. Thus, it is better to act on the gas flow-rate or the pressure.

Figure 9 shows the influence of the residence time on CH_4 conversion and H_2 yield by modifying the gas flow-rate. It is based on experiments 14, 16, and 17, which were carried out at residence times varying between 12 ms and 35 ms, for a constant CH_4 mole fraction of 20% and a temperature of 1740K. Methane conversion increased from 62% to 98% and hydrogen yield increased from 44% to 84% in the range of residence times investigated. This result highlights the predominance of this parameter over the methane mole fraction. At thermodynamic equilibrium, the composition of the C/4H system as a function of temperature shows that the system is composed of solid carbon and molecular hydrogen for a temperature higher than 1500K (Hirsch et al., 2001). Increasing the residence time permits approach to this thermodynamic state equilibrium. A kinetic analysis with the Dsmoke kinetic code (Rodat et al., 2009) showed that a residence time increase improves the reaction extent and reduces the generation of by-products (C_2H_y).

The residence time can also be modified via pressure monitoring. In the experiment presented in Figure 7, the pressure inside the tubes was fluctuated periodically in order to show the effect of pressure variations on the chemical conversion. The reactor pressures presented variations of about 5 kPa with a mean value at 30 kPa. As a consequence, CH_4 and H_2 mole fractions varied with the same frequency. The variation of the residence time was induced by the pressure variations. The highest pressures led to the highest H_2 and the lowest CH_4 mole fractions in the off-gas, because the gas residence time increased slightly, and thus the chemical conversion was enhanced. A pressure increase of 17% (5 kPa) implies a residence time variation of the same order of magnitude and a CH_4 conversion increase of 7%.

3.4. Influence of the temperature

Figure 8 presents the data from two sets of experiments with two different tube temperatures (1670K and 1740K). For a given CH_4 mole fraction of 10%, CH_4 conversion was 59% at 1670K and 81% at 1740K, while H_2 yield was 42% at 1670K and 63% at 1740K. The higher the temperature, the higher the CH_4 conversion and the H_2 yield. As shown in Table 3, the production of acetylene and also ethene is favored at low temperature, corroborating the idea of an incomplete reaction. The methane cracking reaction is endothermic and so increasing the temperature increases the reaction rate.

The selectivity of hydrogen, Z, can be defined as the following ratio:

$$Z=\frac{Y_{H_2}}{X_{CH_4}}. \quad (8)$$

High values of Z mean that most of the methane was converted into hydrogen; the converse is also true. The mean Z was 0.69 and 0.75 at 1670K and 1740K, respectively. Thus, increasing the temperature permits one to limit the formation of by-products.

Figure 6 shows that the H_2 mole fraction in the off-gas slightly increases from 50 s to 600 s, whereas the temperature given by the pyrometer tends to decrease (this temperature decrease is due to the quartz window overheating, which reduces the window transmissivity; thus, the incoming solar flux is slightly decreased). The H_2 mole fraction increase could be the result of an auto-catalytic effect. The CB particles formed could be responsible for this catalysis effect by creating additional reaction sites. Moreover, a slight increase of the pressure and of the available surface area in the tubes due to the carbon deposition could also contribute to the augmentation of the hydrogen production.

The type of carbon deposit forming on the reactor walls also appeared to be temperature dependent. Two types of carbon deposit were observed, corresponding to the insulated zone and to the irradiated zone of the tubes. On the one hand, the most important carbon deposit was a thermophoretic deposition due to the decrease of the tube wall temperature through the insulating layers. Over the irradiated portion of the reactor, the temperature of the wall was higher than or equal to that of the gas stream inside the reactor and, therefore, thermophoretic forces are expected to drive particles away from the wall rather than towards the wall. On the other hand, pyrolitic carbon was found in the hottest part inserted in the cavity. By using internal alumina tubes

(configuration D), the pyrolitic carbon deposit on the irradiated portion of the tubes was greatly alleviated, but the thermophoretic deposit was still present (Figure 10). Moreover, tube configuration C helped to delay tube clogging, but it was not possible to quantify the influence of each design on methane conversion.

3.5. 3D thermal simulation of the reactor

In the previous sections, the main experimental results on methane cracking obtained with the 10 kW solar reactor were presented. The influence of the methane mole fraction, the residence time and the temperature was discussed. The definition of the residence time assumes that the temperature is uniform inside the cavity and the reaction zones, as shown by temperature measurements. To confirm this statement, thermal simulations were carried out with Fluent 6.2 software to predict the temperature distribution in the reactor. The 3-dimensional grid made with Gambit was composed of 4,135,433 cells. Different meshes were used, depending on the reactor components. The mesh used was relatively coarse, except for the tubes, where the flow and the reaction have to be considered. This coarse mesh was chosen in order to minimize computational efforts while achieving convergence, and to have the results be independent of the mesh size. A segregated solver was used to solve the equations sequentially. The gas phase was assumed to be ideal. Viscosity, specific heat, and thermal conductivity were functions of the temperature. Data concerning the materials (graphite and insulation layers) were given by manufacturers. The physical properties of the fluids came from different databases (HSC Chemistry 5.1, 2002; Component plus 3.4, 2001).

The main boundary conditions and assumptions are listed below:

- the temperature of the front face and of the upper part of the tubes is fixed at 300K since it is water-cooled,
- the convective heat transfer coefficient is fixed on the outer shell ($h = 20$ W/m² K) (Müller et al., 2008),
- the incoming solar flux is simulated by a uniform diffuse irradiation through the semi-transparent window boundary (flux density of 2,000 kW/m²); no flux profile is used, but the same average flux exists at any point on the window.
- the operating pressure in the tubes is 40 kPa and the inlet gas temperature is 300K; for these conditions, the gas velocity inlet is 14.76 m/s (4 NL/min) with a CH_4 mole fraction of 0.2.
- concerning the reaction kinetic, an Arrhenius law is selected with parameters permitting the simulation to reach a complete reaction, in order to account for the effect of the gas mixture composition ($k_0=2\ 10^{10}$ s^{-1} and $E_a=281$ kJ/mol).

Simulation results show that the maximum temperature is 2160K in the cavity (Figure 11), while the maximum temperature of the inner tubes is 2120K (Figure 12). As expected, the spatial distribution of temperature in the cavity (tubes and fluid zones) is quite homogeneous. The temperature of the four tubes inside the cavity is uniform, which allows for efficient gas heating. The temperature of the outer reactor shell remains around 300K, which means that the insulation is efficient. Figure 13 shows the temperature of the reactive gas flowing in the tubes and of the inner and outer tubes as a function of the y-coordinate (the distance from the bottom of the tubes). It confirms that the gas temperature and the tube wall temperature are similar in the zone corresponding to the graphite cavity. For higher y-values where the thermophoretic deposit was effectively observed, the gas temperature inside the tubes is higher than the wall temperature. It must be noted that insulation layers were not at steady state during experiments and the temperature in the insulating zone was lower, intensifying the thermophoretic effect.

According to a thermal balance given by the model, approximately 60% of the entering solar power (12,700 W) is IR-radiated outside the cavity through the quartz window. The model does not take into account absorption by the quartz window, which is negligible at 1.38 μm (maximum wavelength of emission of a black-body at 2100K, according to Wien's law). The value given by the manufacturer is about 0.005 cm^{-1}. The power lost through the walls amounts to 35% of the entering solar power, especially through the aluminum front face, which is refrigerated (20% of the entering solar power). The remaining power is evacuated by the gas flow. For the simulation conditions (3.2 NL/min of methane), the theoretical power needed for the reaction of complete cracking, defined as $F_{0,CH_4}.\Delta H_{Reactants(298K)\rightarrow Products(Treactor)}$, amounts to 515 W for a mean reactor temperature of 2000K. This power quantifies the fraction of the absorbed solar power dedicated to the reaction enthalpy, which represents 4% of the entering power. This efficiency does not take into account the sensible enthalpy needed to heat the inert gas (12.8 NL/min), which would lead to a higher thermal efficiency (about 7%). The reactor efficiency can especially be optimized by improving two points. First, thermal losses at the water-cooled front face could be limited with more efficient insulation. Second, IR-radiation from the cavity could be diminished with a higher concentration ratio (e.g., by using a secondary concentrator), which would enable a decrease in the aperture size. Selective windows with high transmissivity in the solar spectrum and high reflectivity in the IR spectrum can further lead to an increase in the energy absorption efficiency, which in turn results in a higher thermal efficiency (Hirsh et al., 2004).

Experimental measurements indicated a lower temperature of the cavity than that predicted by the model. The measured temperature of the tubes was between 1670K and 1770K for the experimental conditions

tested. It can be explained by additional thermal losses in the real reactor configuration. Indeed, the reactor is equipped with 4 sighting portholes for pyrometric measurements. The energy evacuated is estimated to be 600 W, thanks to the Stefan-Boltzmann law that gives the total power radiated by a blackbody at a given temperature, 1700K in the present case. The window is also swept by a nitrogen flow in order to avoid overheating (N_2 flow-rate: 20 NL/min, inlet temperature: 300K, outlet temperature: 800K). The corresponding thermal loss amounts to about 220 W. Neither the sighting portholes nor the nitrogen flow were considered in the model. Nevertheless, the simulation gave an assessment of the thermal behavior of the reactor. A homogeneous cavity temperature was confirmed. It was also demonstrated that the temperature of the gas was close to that of the tube walls, which allowed the assimilation of the reaction temperature to the temperature given by the pyrometer.

4. Conclusion

A 10 kW solar reactor prototype was developed for the co-production of hydrogen and carbon black from thermal methane cracking. An experimental study was conducted to determine reactor performances as a function of operating conditions. Experimental results showed a maximum CH_4 conversion of 98% and an H_2 yield of 90% for a cavity wall temperature of 1770K, a residence time of 32 ms and a CH_4 mole fraction of 10%. Two main parameters appeared to be of great importance on the chemical conversion: the residence time and the temperature. The latter parameter was also investigated through simulations. The cavity temperature was quite homogeneous, with the most important thermal loss being IR-radiation through the window. It was also possible to confirm the presence of a temperature gradient responsible for thermophoretic carbon deposition toward the reactor exit. The simulation showed that the gas temperature is equal to the wall temperature in the irradiated part of the tubes, but the gas is hotter than the walls in the insulated section, leading to thermophoretic carbon deposition on the wall.

Future experiments will focus on the production of larger quantities of CB in order to determine its properties. The numerical model will be improved in order to estimate real kinetic parameters.

Acknowledgements

This study was funded by the European Project Solhycarb (2006-2010, Contract SES-CT2006-19770). The authors wish to thank Olivier Prévost, Marc Garrabos and Emmanuel Guillot for their technical support during the solar reactor manufacturing and the experimental campaigns.

Nomenclature

E_a activation energy (J/mol)

F total molar flow-rate (mol/s)

F_i molar flow-rate of species i (mol/s)

$F_{0,i}$ inlet molar flow-rate of species i (mol/s)

h convection coefficient (W/m² K)

ΔH° standard reaction enthalpy (J/mol)

k_0 pre-exponential factor or frequency factor (s^{-1})

P absolute pressure (Pa)

P_0 absolute pressure at the tube entrance (Pa)

P_{solar} solar power input (W)

Q_0 inlet gas flow rate (m^3/s)

r reaction rate (mol/m^3 s)

R universal gas constant (8.314 J/mol K)

T absolute temperature (K)

T_0 absolute temperature at the tube entrance (K)

V_r reactor volume (m^3)

X_{CH_4} methane conversion

y_i mole fraction of species i

Y_{H_2} hydrogen yield

Greek letters:

α chemical expansion factor ($\frac{1}{1+\frac{F_{Ar}}{F_{0,CH_4}}}$)

β physical dilatation factor ($\frac{P_0 T}{P T_0}$)

τ mean residence time ($\frac{V_r}{Q_0}$ (s))

References

Abanades, S., Flamant, G., 2007. Experimental study and modeling of a high-temperature solar chemical reactor for hydrogen production from methane cracking. Int. J. Hydrogen Energy 32(10-11), 1508-1515.

Abanades, S., Flamant, G., 2008. Hydrogen production from solar thermal dissociation of methane in a high-temperature fluid-wall chemical reactor. Chemical Engineering and Processing: Process Intensification 47(3), 490-498.

Adams, R., 2007. Booming world carbon black demand but price rises fail to keep pace with rising gas & feedstock costs. Focus on Pigments 3, 1-2.

Barreto, L., Makihira, A., Riahi, K., 2003. The hydrogen economy in the 21st century: a sustainable development scenario. Int. J. Hydrogen Energy 28(3), 267-284.

Component Plus 3.4, 2001, Pro Sim, France.

Dahl, J.K., Buechler, K.J., Weimer, A.W., Lewandowski, A., Bingham, C., 2004a. Solar-thermal dissociation of methane in a fluid-wall aerosol flow reactor. Int. J. Hydrogen Energy 29(7), 725-736.

Dahl, J.K., Buechler, K.J., Finley, R., Stanislaus, T., Weimer, A.W., Lewandowski, A., Bingham, C., Smeets, A., Schneider, A., 2004b. Rapid solar-thermal dissociation of natural gas in an aerosol flow reactor. Energy 29(5-6), 715-725.

Gonzalez-Aguilar, J., Dème, I., Fulcheri, L., Flamant, G., Gruenberger, TM., Ravary, B., 2004. Comparison of simple particle–radiation coupling models applied on a plasma black process. Plasma Chemistry and Plasma Processing 24(4), 603–23.

Guéret, C., Billaud, F., 1994. Thermal coupling of methane: influence of hydrogen at 1330°C. Experimental and simulated results. J. Anal. Appl. Pyrolysis 29(2), 183–205.

Hirsch, D., Epstein, M., Steinfeld, A., 2001. The solar thermal decarbonization of natural gas. Int. J. Hydrogen Energy 26(10), 1023-1033.

Hirsch, D., Steinfeld, A., 2004. Solar hydrogen production by thermal decomposition of natural gas using a vortex-flow reactor. Int. J. Hydrogen Energy 29(1), 47-55.

Holmen, A., Olsvik, O., Rokstad, O.A., 1995. Pyrolysis of natural gas: chemistry and process concepts. Fuel Processing Technology 42(2-3), 249-267.

HSC Chemistry 5.1, 2002, Outokumpu Research Oy, Pori, Finland.

Kogan, M., Kogan, A., 2003. Production of hydrogen and carbon by solar thermal methane splitting. I. The unseeded reactor. Int. J. Hydrogen Energy 28(11), 1187-1198.

Kogan, A., Kogan, M., Barak, S., 2004. Production of hydrogen and carbon by solar thermal methane splitting. II. Room temperature simulation tests of seeded solar reactor. Int. J. Hydrogen Energy 29(12),1227-1236.

Kogan, A., Kogan, M., and Barak, S., 2005. Production of hydrogen and carbon by solar thermal methane splitting. III. Fluidization, entrainment and seeding powder particles into a volumetric solar receiver. Int. J. Hydrogen Energy 30(1), 35-43.

Mason, J. E., 2007. World energy analysis: H_2 now or later?. Energy Policy 35(2), 1315-1329.

Müller, R., Lipiński, W., Steinfeld, A., 2008. Transient heat transfer in a directly-irradiated solar chemical reactor for the thermal dissociation of ZnO. Applied Thermal Engineering 28(5-6), 524-531.

Muradov, N., 2001a. Hydrogen via methane decomposition: an application for decarbonization of fossil fuels. Int. J. Hydrogen Energy 26(11), 1165-1175.

Muradov, N., 2001b. Catalysis of methane decomposition over elemental carbon. Catalysis Communications 2(3-4), 89-94.

Muradov, N., Chen, Z., Smith, F., 2005a. Fossil hydrogen with reduced CO_2 emission: Modeling thermocatalytic decomposition of methane in a fluidized bed of carbon particles. Int. J. Hydrogen Energy 30(10), 1149-1158.

Muradov, N., Veziroglu, T. N., 2005b. From hydrocarbon to hydrogen–carbon to hydrogen economy. Int. J. Hydrogen Energy 30(3), 225-237.

Rodat, S., Abanades, S., Coulié, J., Flamant, G., 2009. Kinetic modelling of methane decomposition in a tubular solar reactor. Chem. Eng. J. 146(1), 120-127.

Trommer, D., Hirsch, D., Steinfeld, A., 2004. Kinetic investigation of the thermal decomposition of CH_4 by direct irradiation of a vortex-flow laden with carbon particles. Int. J. Hydrogen Energy 29(6), 627-633.

Wyss, J., Martinek J., Kerins, M., Dahl, J.K., Weimer, A., Lewandowski, A., Bingham, C., 2007. Rapid Solar-thermal Decarbonization of Methane in a Fluid-wall Aerosol Flow Reactor – Fundamentals and Application. Int. J. Chem. Reactor Engineering, 5, A69.

Table 1: Insulating materials properties

Insulating material 1		Insulating material 2		Insulating material 3	
Maximum temperature	>3273 K	1873 K		1273 K	
Temperature (K)	Thermal conductivity (W/m-K)	Temperature (K)	Thermal conductivity (W/m-K)	Temperature (K)	Thermal conductivity (W/m-K)
1673	0.429	1273	0.18	473	0.022
1873	0.53	1473	0.25	673	0.025
2173	0.824	1673	0.35	873	0.035
2473	1.298	1873	0.48	1073	0.044

Table 2: Experimental conditions

Run N°	Ar(NL/min)	CH_4(NL/min)	CH_4 mole fraction (%)	Pressure (Pa)	$T_{pyrometer}$ (K)	Configuration	Residence time (s)
1	10.8	1.2	10.00	40000	1770	4A	0.032
2	16	4	20.00	38000	1770	4A	0.018
3	16	4	20.00	35000	1770	4A	0.017
4	20	4	16.67	35000	1770	4A	0.014
5	16	4	20.00	32000	1700	4B	0.018
6	16	6	27.27	35000	1710	4B	0.017
7	16	6	27.27	25000	1710	4B	0.012
8	10.8	1.2	10.00	30000	1670	2A+2C	0.027
9	16	8	33.33	30000	1670	2A+2C	0.013
10	18	2	10.00	30000	1670	2C+2D	0.018
11	16	4	20.00	30000	1670	2C+2D	0.018
12	14	6	30.00	30000	1670	2C+2D	0.018
13	18	2	10.00	30000	1740	4D	0.018
14	16	4	20.00	30000	1740	4D	0.018
15	14	6	30.00	30000	1740	4D	0.018
16	24	6	20.00	30000	1740	4D	0.012
17	8	2	20.00	30000	1740	4D	0.035

Table 3: Main results corresponding to the experimental conditions of Table 2

Run N°	CH_4 conversion (%)	H_2 yield (%)	Off-gas composition (mole fraction)					Thermochemical efficiency (%)
			H_2	CH_4	C_2H_4	C_2H_6	C_2H_2	
1	98	90	0.1625	0.0018	0.0004	0.0000	0.0202	1.14
2	92	74	0.2518	0.0138	0.0006	0.0000	0.0392	3.56
3	97	76	0.2555	0.0055	0.0006	0.0000	0.0417	3.75
4	94	75	0.2170	0.0090	0.0005	0.0000	0.0302	3.64
5	83	59	0.2056	0.0294	0.0012	0.0001	0.0398	3.11
6	85	64	0.2925	0.0340	0.0036	0.0002	0.0530	4.80
7	67	47	0.2278	0.0790	0.0041	0.0003	0.0361	3.78
8	75	56	0.1033	0.0227	0.0009	0.0001	0.0207	0.83
9	32	20	0.1230	0.2123	0.0067	0.0007	0.0179	2.36
10	59	42	0.0795	0.0388	0.0020	0.0002	0.0160	1.09
11	61	40	0.1480	0.0727	0.0032	0.0002	0.0282	2.25
12	62	43	0.2270	0.1000	0.0043	0.0003	0.0426	3.43
13	81	63	0.1177	0.0173	0.0006	0.0000	0.0258	1.55
14	83	61	0.2173	0.0307	0.0011	0.0000	0.0448	3.17
15	78	58	0.2943	0.0560	0.0021	0.0001	0.0536	4.46
16	62	44	0.1617	0.0703	0.0032	0.0002	0.0264	3.55
17	98	84	0.2523	0.0037	0.0003	0.0000	0.0187	1.87

Figure captions

Figure 1: Design of the 10 kW solar reactor prototype

Figure 2: Cross section scheme for tube configurations A, B, and C (sizes are in mm, not scaled)

Figure 3: Scheme of the 1 MW solar furnace

Figure 4: Temperature measurement

Figure 5: Time course of temperatures

Figure 6: CH_4 and H_2 mole fractions in the off-gas and tube temperature (runs 3 and 4)

Figure 7: CH_4 and H_2 mole fractions in the off-gas and reactor pressure (runs 13, 14 and 15)

Figure 8: Results of CH_4 conversion and H_2 yield versus CH_4 mole fraction for a constant residence time of 18 ms at two different temperatures (runs 10, 11, 12, 13, 14 and 15)

Figure 9: Results of CH_4 conversion and H_2 yield versus residence time at 1740K for a constant CH_4 mole fraction (runs 14, 16 and 17)

Figure 10: Photograph of the thermophoretic deposit on the internal alumina tubes

Figure 11: Temperature distribution in the reactor (K)

Figure 12: Temperature contours on the tubes (K)

Figure 13: Temperature profiles of the gas and of the inner and outer tubes

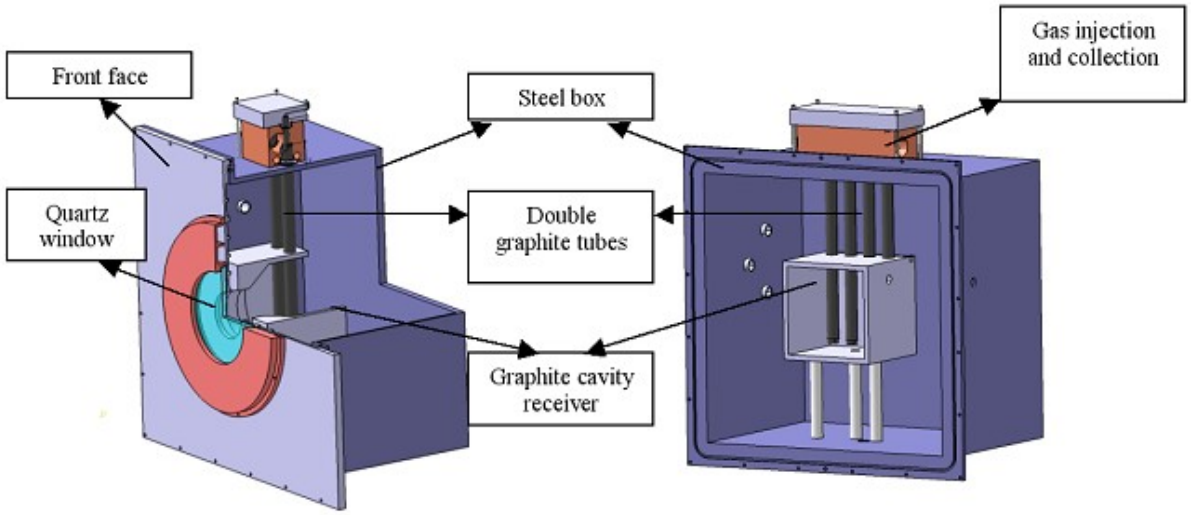

Figure 1: Design of the 10 kW solar reactor prototype

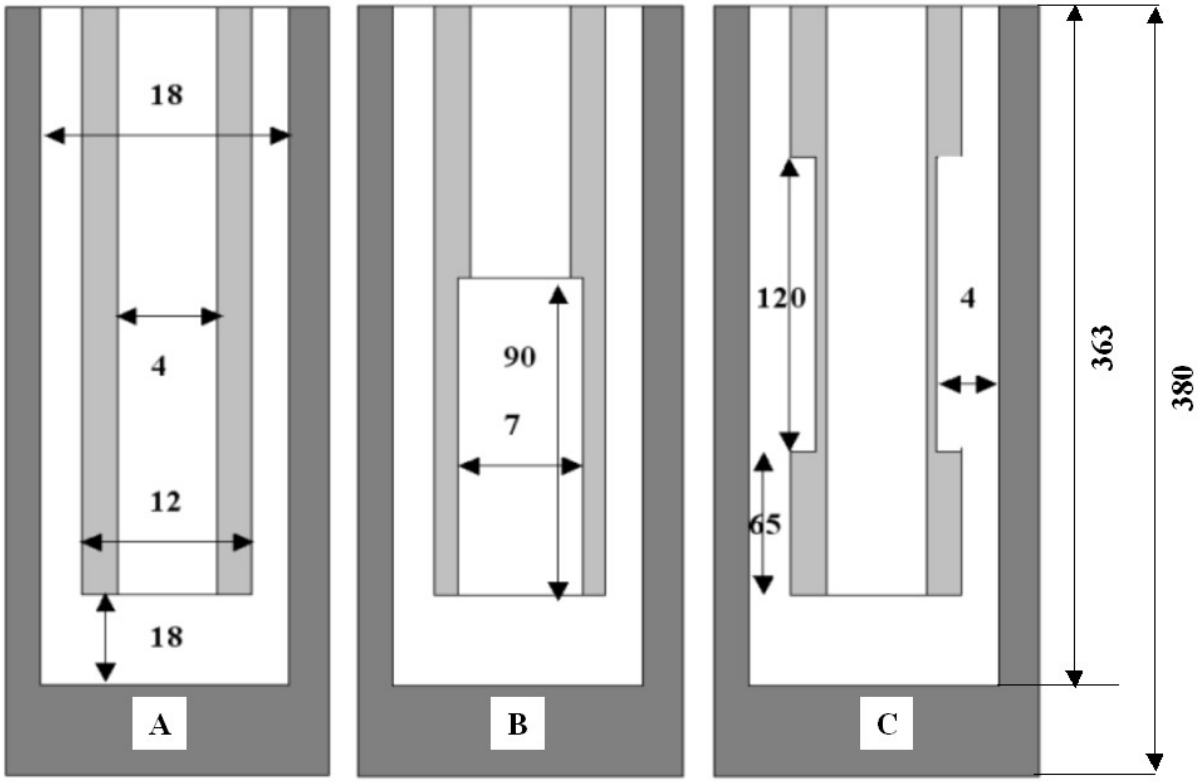

Figure 2: Cross section scheme for tube configurations A, B, and C (sizes are in mm, not scaled)

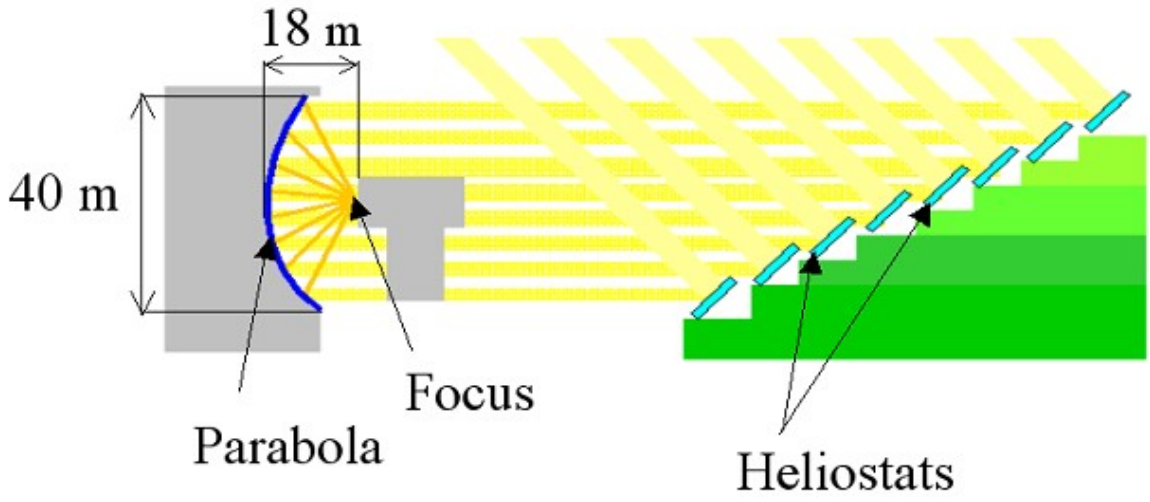

Figure 3: Scheme of the 1 MW solar furnace

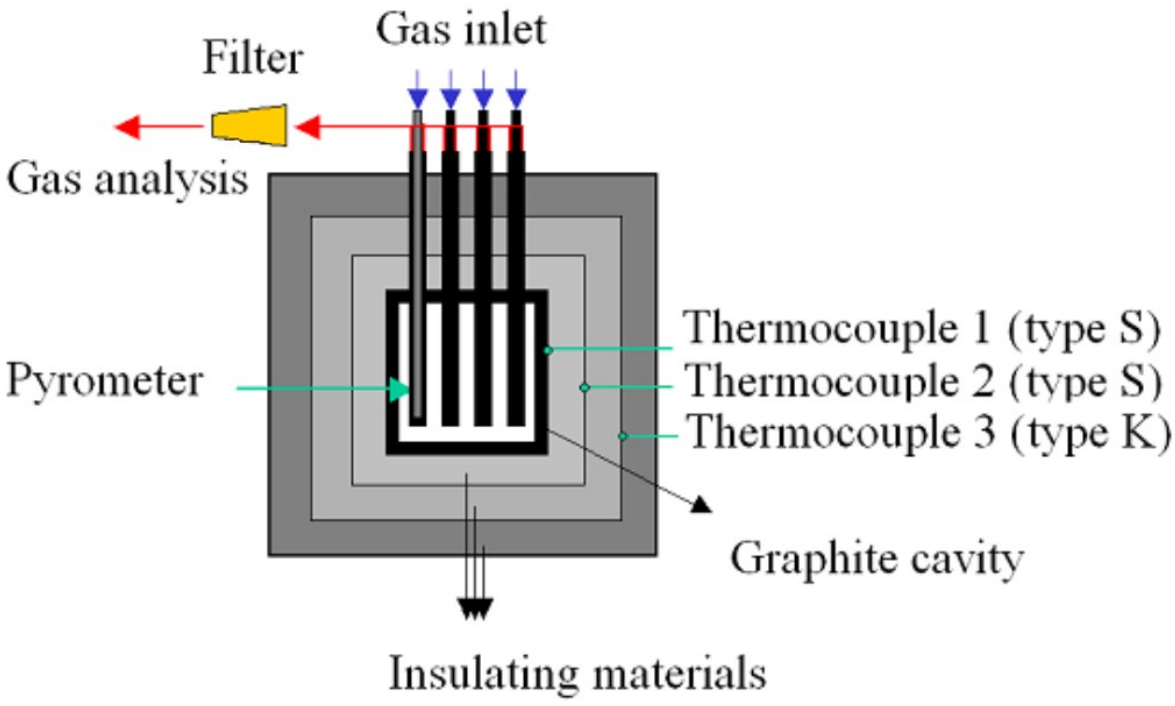

Figure 4: Temperature measurement

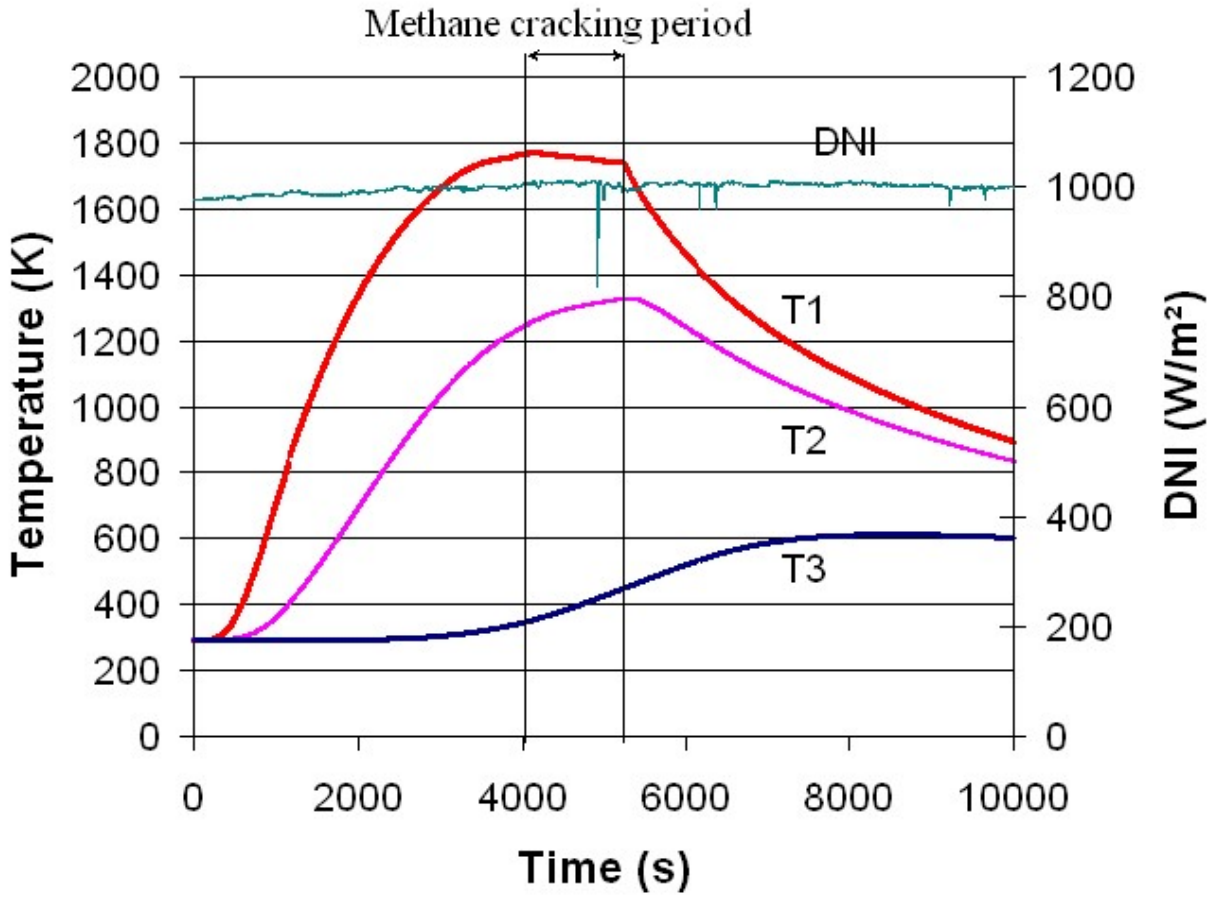

Figure 5: Time course of temperatures

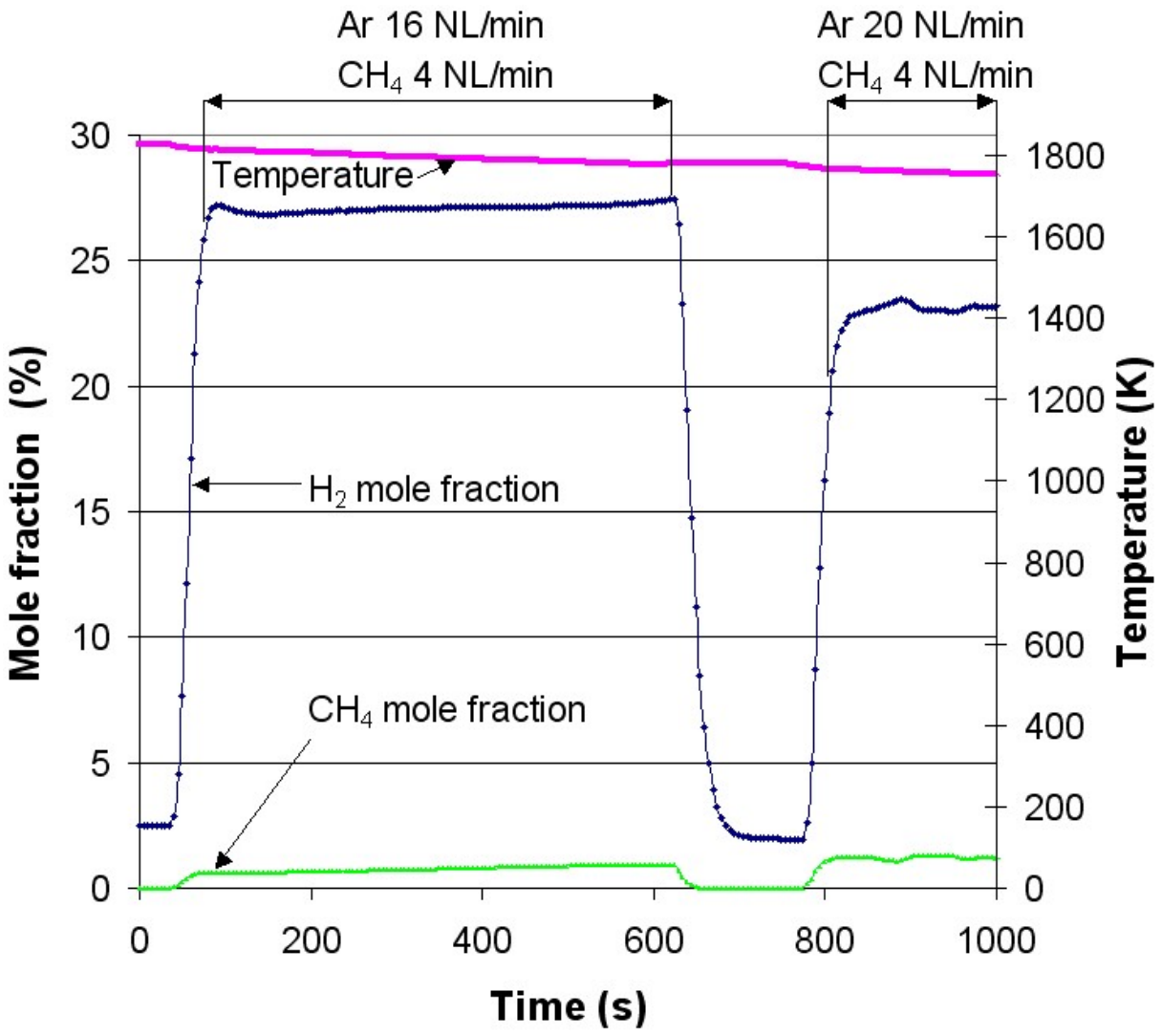

Figure 6: CH_4 and H_2 mole fractions in the off-gas and tube temperature (runs 3 and 4)

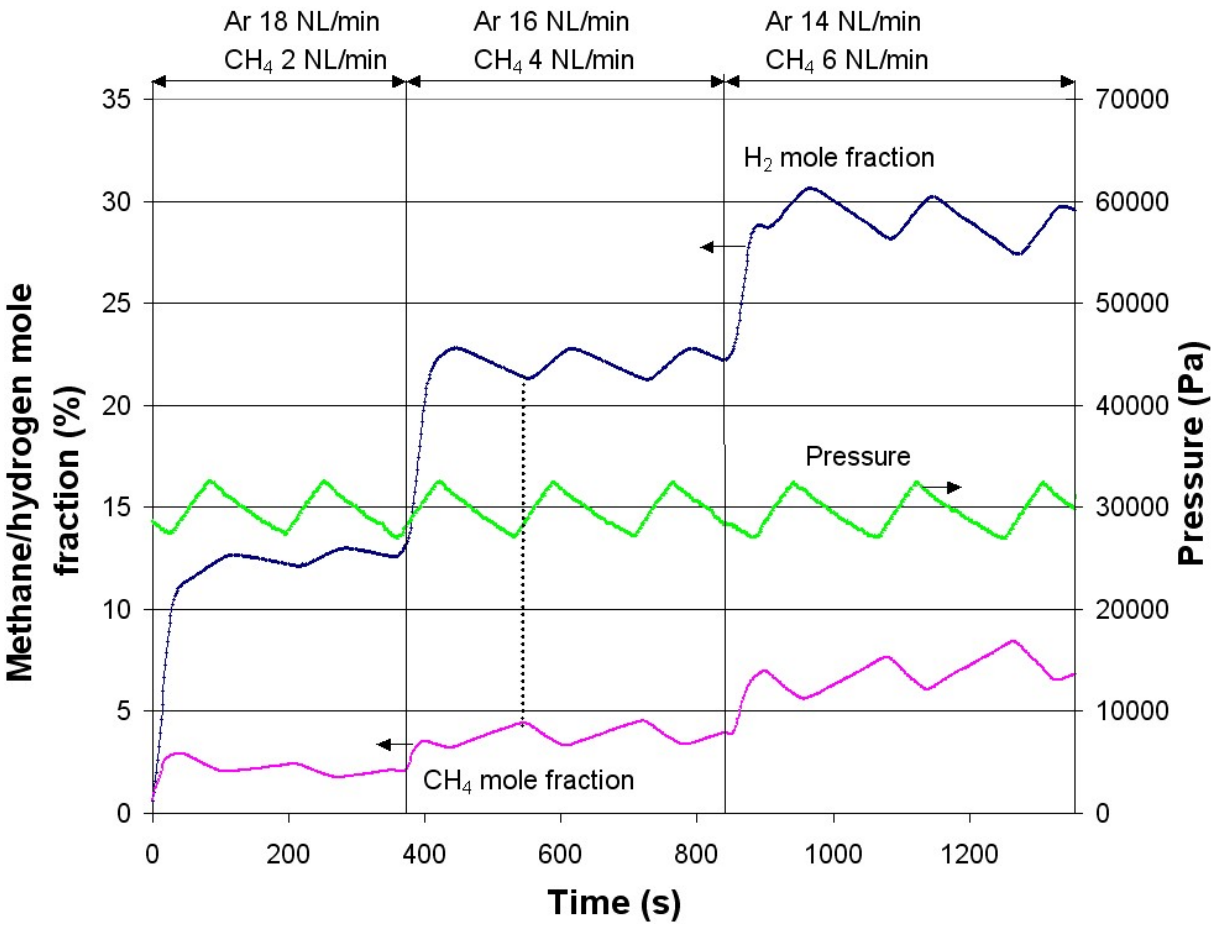

Figure 7: CH_4 and H_2 mole fractions in the off-gas and reactor pressure (runs 13, 14 and 15)

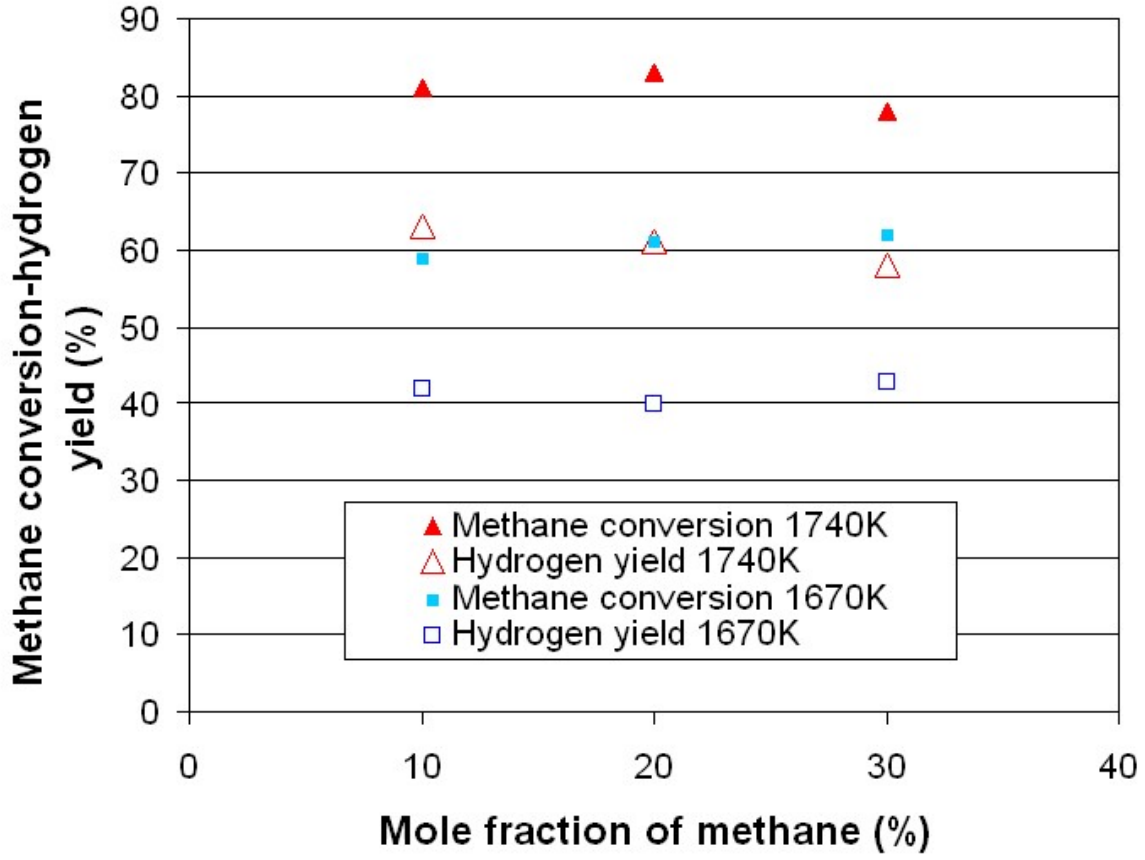

Figure 8: Results of CH_4 conversion and H_2 yield versus CH_4 mole fraction for a constant residence time of 18 ms at two different temperatures (runs 10, 11, 12, 13, 14 and 15)

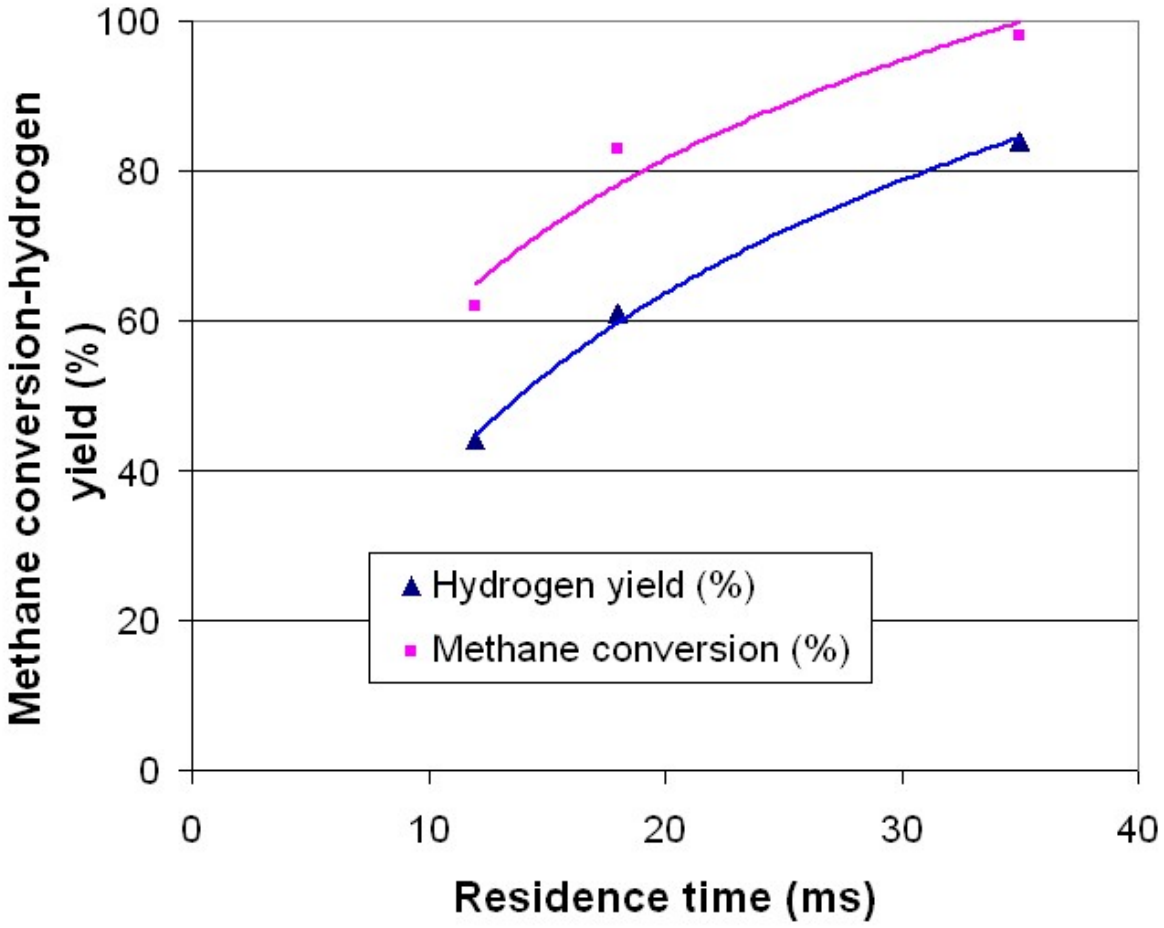

Figure 9: Results of CH_4 conversion and H_2 yield versus residence time at 1740K for a constant CH_4 mole fraction (runs 14, 16 and 17)

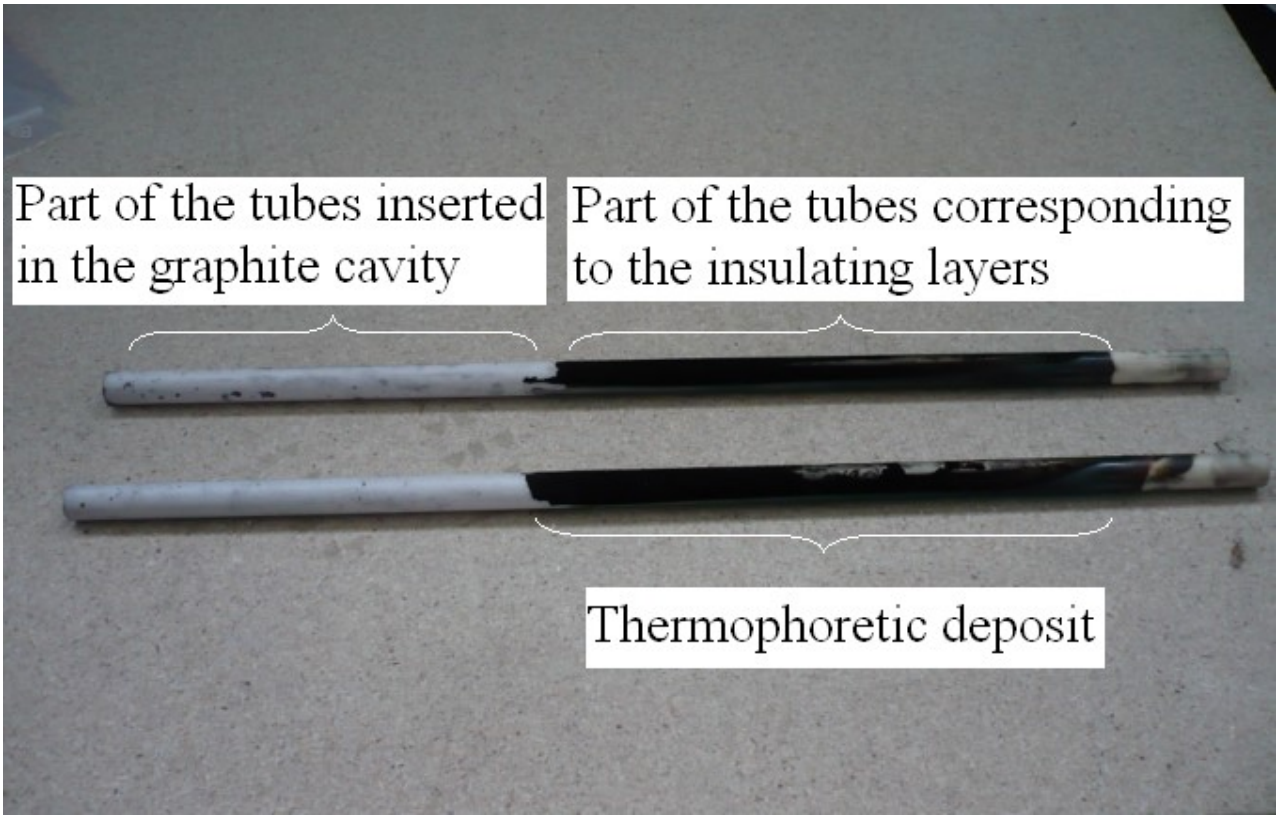

Figure 10: Photograph of the thermophoretic deposit on the internal alumina tubes

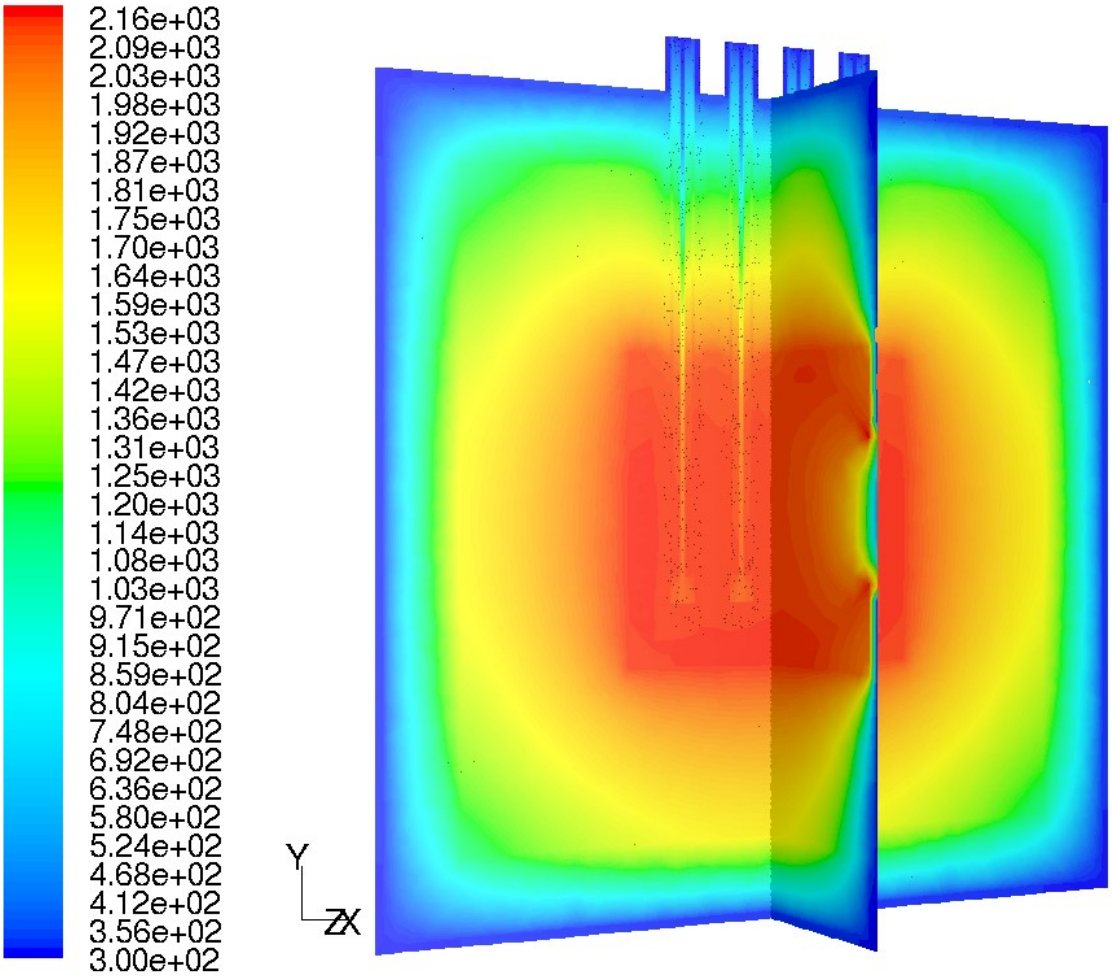

Figure 11: Temperature distribution in the reactor (K)

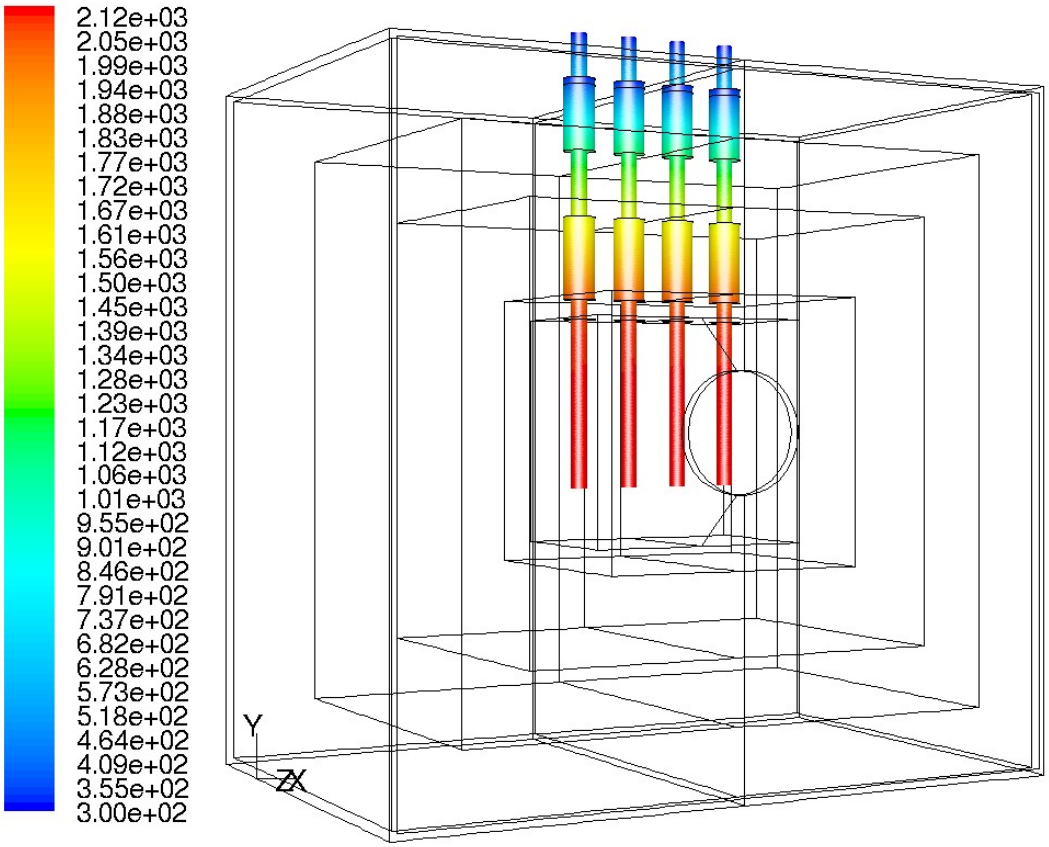

Figure 12: Temperature contours on the tubes (K)

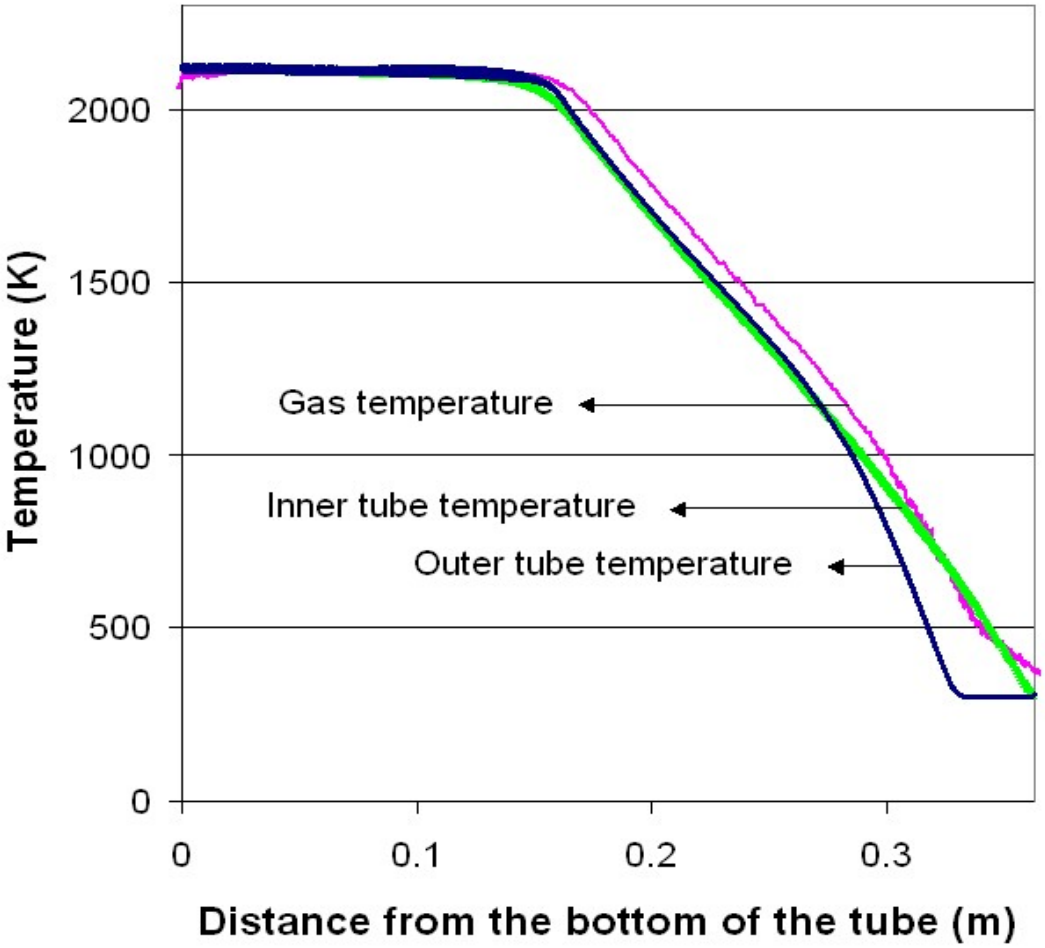

Figure 13: Temperature profiles of the gas and of the inner and outer tubes